Source tracing of thunderstorm generated inertia-gravity waves observed during the RADAGAST campaign in Niamey, Niger

Athreyas, Kashyapa Naren; Gunawan, Erry; Tay, Bee Kiat

2018

Athreyas, K. N., Gunawan, E., & Tay, B. K. (2018). Source tracing of thunderstorm generated inertia-gravity waves observed during the RADAGAST campaign in Niamey, Niger. Journal of Atmospheric and Solar-Terrestrial Physics, 172, 1-9. doi:10.1016/j.jastp.2018.03.003

https://hdl.handle.net/10356/90111

https://doi.org/10.1016/j.jastp.2018.03.003

Available online at www.sciencedirect.com

Journal of Atmospheric and Solar-Terrestrial Physics

Journal homepage: www.elsevier.com/locate/jasts

Source tracing of thunderstorm generated inertia-gravity waves observed during the RADAGAST campaign in Niamey, Niger

Kashyapa Naren Athreyas[a], Erry Gunawan[a], Tay Bee Kiat[b]

[a] *Satellite Research Center, Nanyang Technological University, 637553, Singapore*
[b] *DMERI, DSO National Laboratories, 118225, Singapore*

ARTICLE INFO

Article history:
Received
Received in revised form
Accepted

Keywords:
Inertia gravity waves
Thunderstorms
GROGRAT
West African Climate

ABSTRACT

In recent years, the climate changes and weather have become a major concern which affects the daily life of a human being. Modelling and prediction of the complex atmospheric processes needs extensive theoretical studies and observational analyses to improve the accuracy of the prediction. The RADAGAST campaign was conducted by ARM climate research stationed at Niamey, Niger from January 2006 to January 2007, which was aimed to improve the west African climate studies have provided valuable data for research. In this paper, the characteristics and sources of inertia-gravity waves observed over Niamey during the campaign are investigated. The investigation focuses on highlighting the waves which are generated by thunderstorms which dominate the tropical region. The stratospheric energy densities spectrum is analysed for deriving the wave properties. The waves with Eulerian period from 20 – 40 hours occupied most of the spectral power. It was found that the waves observed over Niamey had a dominant eastward propagation with horizontal wavelengths ranging from 350 – 1400 km, and vertical wavelengths ranging from 0.9 – 3.6 km. GROGRAT model with ERA-Interim model data was used for establishing the background atmosphere to identify the source location of the waves. The waves generated by thunderstorms had horizontal propagation distances varying from 200 – 5000 km and propagation duration from 2 to 4 days. The horizontal phase speeds varied from 2 – 20 m/s with wavelengths varying from 50 – 1500 km, vertical phase speeds from 0.02 – 0.2 m/s and wavelengths from 2 – 15 km at the source point. The majority of sources were located in South Atlantic ocean and waves propagating towards northeast direction. This study demonstrated the complex large scale coupling in the atmosphere.

1. Introduction

The earth's atmosphere is complexly coupled with the lithosphere, outer space and also within the different atmospheric layers (Yiğit & Medvedev 2015). In the last few decades, it was found that energy transport from one atmospheric layer to another has been considered as a significant process which affects the global climate budget (Plougonven & Zhang 2013; Yiğit et al. 2016; Yiğit & Medvedev 2015). Gravity waves have been identified as one of the key components of the atmosphere which acts in distributing the energy and momentum across the different vertical layers and geographical regions. The common sources of gravity waves are mountains, lithospheric movements, convective clouds, frontogenesis and oceans (Fritts & Alexander 2003; Curry & Murty 1974). Tropical gravity waves play a significant role in middle atmospheric circulation and oscillations (Evan et al. 2012). In the tropical region, deep convective clouds/thunderstorms can generate gravity waves which deposit energy and momentum in stratosphere, hence altering the circulation (Lane & Moncrieff 2008; Fritts & Alexander 2003). Deep convection have found to be one of the major sources of gravity waves especially in tropical region where they are predominant (Wang 2005; Lane & Moncrieff 2008; Morrison & Grabowski 2013; Pramitha et al. 2016). Convection can generate gravity waves as a result of three possible mechanisms namely pure thermal forcing, mechanical oscillator effect and obstacle effect (Fritts & Alexander 2003). Pure thermal forcing is a result of convective clouds radiating waves into stably stratified atmosphere above. Mechanical oscillator acts as the physical oscillator which generates the waves. Obstacle effect defines the flow over the convection which is treated as an obstacle similar to orographic wave generation (Salby & Garcia 1987; Fritts & Alexander 2003; Kim et al. 2003; Clarke et al. 1986).

The parameterisation of these waves is important in global circulation models (GCM) which is used for forecasting and analysis of the processes and coupling in the atmosphere. To develop these parameterisations, it is necessary to characterise the gravity waves' properties such as frequency, vertical and horizontal wavelengths, phase velocities and energies etc. and identify the cause of their generation (Fritts & Alexander 2003; Lane & Moncrieff 2008). In order to retrieve the gravity wave properties, over the years, numerous studies have presented the methods to observe the gravity wave in the atmosphere using various instruments such as hodograph, radar, lidar, satellite images and radiosondes. Various signal processing techniques such as Fourier analysis and wavelet transform have been applied to observe the properties (Eckermann & Vincent 1989; Fritts & Alexander 2003).

Active gravity wave properties were studied using the TWP-ICE campaign data which covered stations near the northwest Australian region (Evan & Alexander 2008; Evan et al. 2012; Hankinson et al. 2014b; Hankinson et al. 2014a). Observational studies have been carried with data collected at various locations such as (Hima Bindu et al. 2016; Pramitha et al. 2016; Pramitha et al. 2015) in the Indian subcontinent, (Chun & Baik 1998; Wang & Zhang 1999; Lane & Moncrieff 2008; Jewtoukoff et al. 2013; Plougonven et al. 2015) in the North American continent and various others which are not cited in the article, but few studies have been focused on the west African region.

The western African monsoon region represents a unique geographical system being surrounded by ocean, vegetation and a large desert land which leads to unique meteorological behaviour. Kafando et al. (2008) showed the different frequencies of gravity waves present in the region using radiosonde data. Gravity waves structures were correlated with the thunderstorms in west African region using a 10 year infrared sound stations (Blanc et al. 2014). Variation and characteristics of the gravity waves generated during the monsoon season were studied using several radiosonde stations covering western Africa which provided much clear picture of the mesoscale waves generated by convection (Kafando et al. 2016). The waves identified by these studies have mean horizontal and vertical wavelengths of 2000 km and 2 km. These observational studies provided general idea regarding the waves associated with convective environment for this region. However, these

studies do not emphasise on the particular location of the sources associated with thunderstorms, which is the motivation of our study.

This paper is focused on characterising the gravity waves which are observed during RADAGAST campaign conducted by ARM (Atmospheric Radiation Measurement) and identifying their sources. The profiles of temperature and wind speed are used for spectral analysis and deriving the gravity wave properties in the stratosphere (from 19 – 23 km altitude). The identified waves are analysed to determine their origin with ray tracing method. The rest of the article is organised as follows: section 2 discusses the data used and background atmosphere calculation. Section 3 explains the methodology used to identify and retrieve the gravity wave properties along with the obtained results. Section 4 describes the ray tracing method briefly and discusses the simulation results and identified sources of the waves analysed.

2. Data

The radiosonde data used in this study was obtained from ARM facility in Niamey, Niger (13.47° N, 2.17° E), collected during the RADAGAST campaign from January 2006 to January 2007. The geographical location and close up of the Niamey city is shown in Figure 1. The climate is characterised clearly by two seasons – dry and wet. The dry season extends from October to April which experiences dust and sandstorms while the wet season extends from May to September with strong daily precipitations (Kafando et al. 2016; Kafando et al. 2008). Vertical profiles of temperature, wind speed and direction, were retrieved from MERGESONDE data product which assimilates the radiosonde, high-resolution microwave radiometer data with interpolated model data. The vertical profiles are produced at 315 altitude levels between 0-60 km with a temporal resolution of 60 s (Troyan 2012). The variation in temperature and wind speed components in horizontal plane during the campaign is shown in Figure 2.

The study was limited to analyse up till the altitude of 23 km for investigating the gravity wave presence because the data does not provide the variables consistently in the stratosphere above 23 km. Though, this reduced the total number of profiles that could be used, the required temporal resolution was still retained. The data was analysed monthly in order to monitor the variation of gravity wave properties as the season varies along these months. Therefore, the mean background state was calculated for each month by averaging the time series. The mean vertical profiles of temperature ($\bar{T}$), horizontal components of wind speed, zonal ($\bar{u}$) and, meridional ($\bar{v}$) are shown for wet season months in Figure 3. The mean state of zonal wind varies quite widely for different months, while the monthly mean meridional wind variation is relatively small.

From the temperature profiles in Figure 2 and Figure 3, it is possible to deduce that the tropopause occurs approximately at 16 km by analysing the sharp gradient change (seen by dark blue patch along the time series). It is important to identify the tropopause as the inversion layer is to be avoided in the spectral analysis which can lead uncertainties.

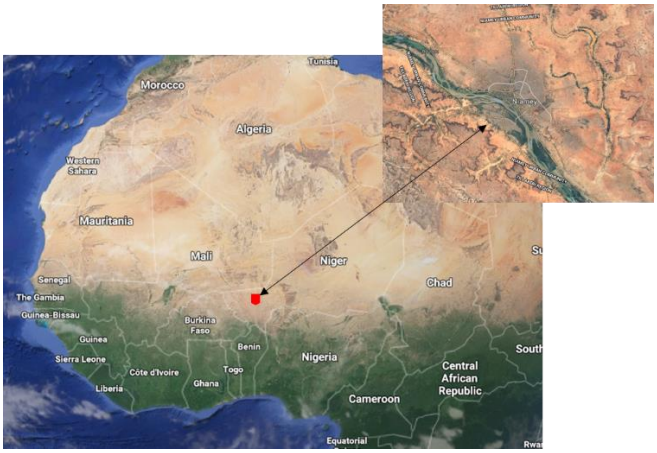

Figure 1: Location of Niamey, Niger where the RADAGAST campaign was conducted.

The gravity wave analysis is performed assuming the perturbation theory in which the variables are separated into background mean state (constant or very slowly varying) and perturbation (deviation from the mean state). The perturbations of the variables are defined as the departure from the mean state and can be expressed as:

$$\begin{aligned} u' &= u - \bar{u} \\ v' &= v - \bar{v} \\ T' &= T - \bar{T} \end{aligned} \tag{1}$$

The primers represent the perturbations, while the regular variable notations represent the true value of the variable. It is convenient to use such an approach because the perturbations clearly highlight any wave kind of behaviour in the signals. Several studies have applied this approach in order to identify the gravity wave signatures in the observations (Evan & Alexander 2008; Geller & Gong 2010; Hankinson et al. 2014b; Pramitha et al. 2016). The study uses monthly mean state to analyse the pertubations on a monthly basis.

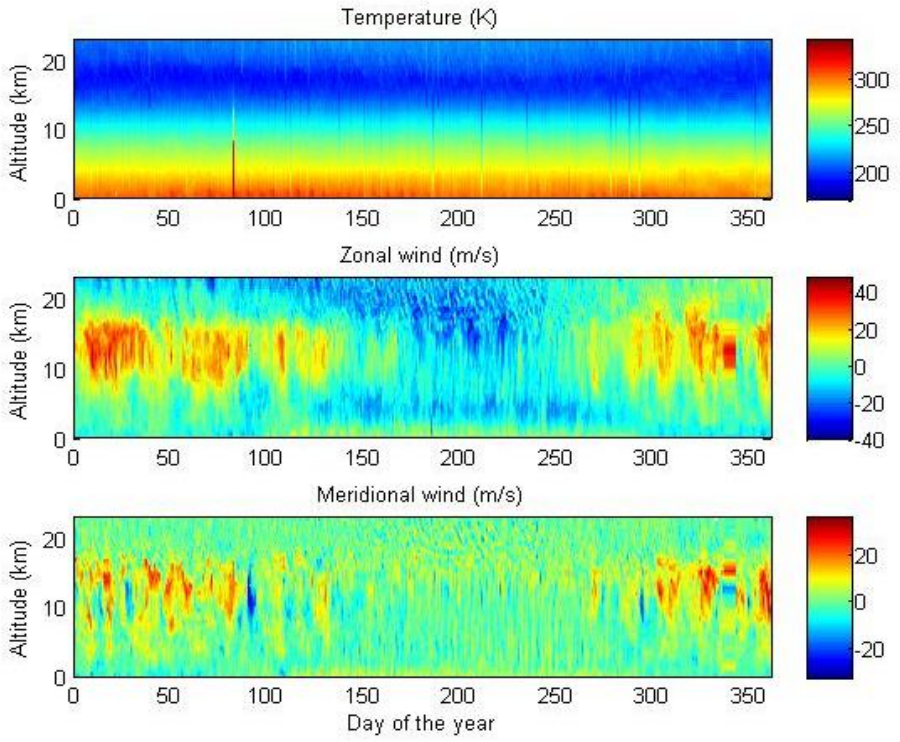

Figure 2: Time-altitude plots of temperature, zonal and meridional wind speed during the RADAGAST campaign above Niamey, Niger.

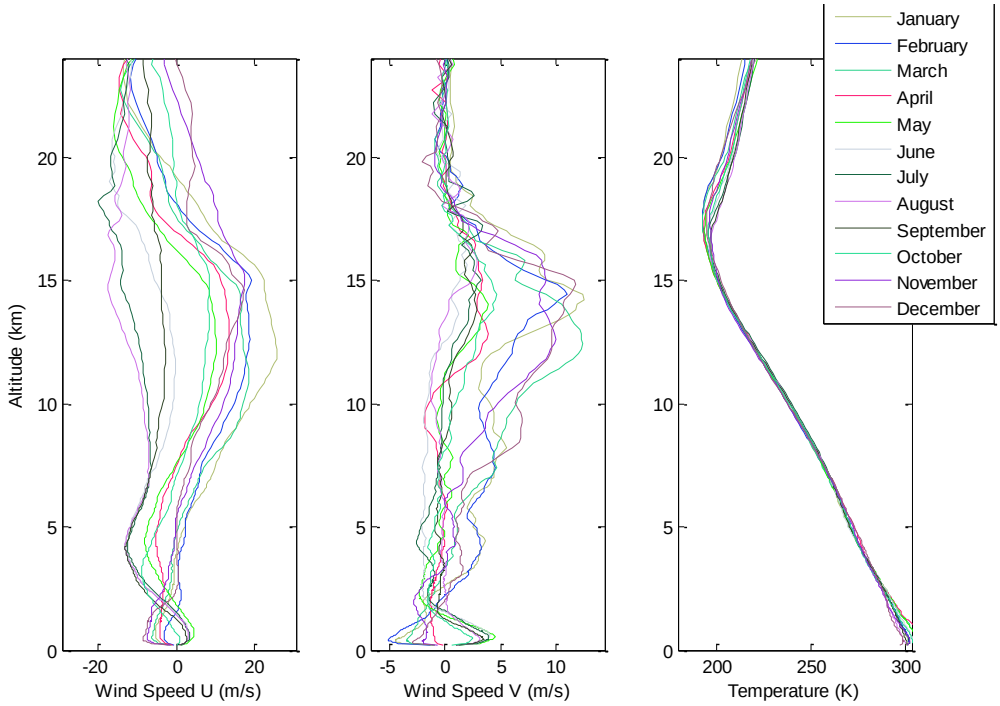

Figure 3: Monthly mean vertical profiles of zonal, meridional wind speed and temperature during the RADAGAST campaign at Niamey.

3. Inertia-Gravity wave properties

One of the common methods to identify and investigate the waves present in any signal is to analyse the spectrum. Inertia gravity wave scales are defined as the frequencies which are closer to earth's inertial frequency f_e and much lower than the buoyancy frequency N (Fritts & Alexander 2003). The expressions for f_e and N are shown in equations (2) and (3).

$$f_e = 2\Omega sin\Theta \tag{2}$$

$$N = \sqrt{\frac{g}{T}\left(\frac{dT}{dz} + \Gamma_d\right)} \tag{3}$$

where Ω is the Earth's angular velocity in Hz, Θ is the latitude in radians, g is the acceleration due to gravity in m/s^2, Γ_d is the dry adiabatic lapse rate and z is the vertical axis distance. The inertial frequency of earth for Niamey was calculated to be $3.397 \times 10^{-5} Hz$ and buoyancy frequency at 23 km was $0.024\ Hz$. It is to be noted that using MERGESONDE data with only horizontal velocity data, it is not possible to identify high frequency gravity waves which have periods closer to N. Previous studies suggest that spectrum of horizontal kinetic energy can be used to identify the Eulerian frequencies (scales) ω of inertia gravity waves present in the signal (Geller & Gong 2010). The perturbations u',v' amd T' can be used to obtain the horizontal kinetic and potential energy densities E_k and E_p. Equations (4) and (5) show the expressions for E_k and E_p:

$$E_k = \frac{1}{2}\left(u'^2 + v'^2\right) \tag{4}$$

$$E_p = \frac{1}{2}\frac{g^2}{N^2}\left(\frac{T'}{T_m}\right)^2 \tag{5}$$

where T_m is the mean temperature. In this study, the waves present in stratosphere are studied and characterised. As mentioned previously, the tropopause above Niamey occurs approximately at 16 km. therefore, the profiles are analysed in between 19 – 23 km in order to avoid the inversion layer uncertainties.

The time series signals of u'^2 and v'^2 are averaged in stratosphere altitude range and analysed using wavelet transform and then summed for wavelet analysis to E_k which is shown in Figure 4. A complex wavelet analysis is used to investigate the scales of waves which can be categorised as inertia-gravity waves. The complex Morlet wavelet was used for the transformation into frequency-time domain. It is a complex nonorthogonal wavelet which is commonly used to analyse the time series signals, especially in the atmospheric studies (Torrence & Compo 1998; Hankinson et al. 2014b). The wavelet transforms of individual velocity series are summed to obtain the spectrum of energy density shown in equation (4) which is analysed in order to extract wave information. There are some key properties we need to retrieve following ω in order to characterise the gravity waves and these properties are intrinsic frequency $\hat{\omega}$ (Lagrangian frequency), horizontal and vertical wavenumbers k, l, m. With these properties, it is possible to characterise their scale and direction of propagation. The frequency-time wavelet spectrum for the month of May is shown in Figure 4 as an example.

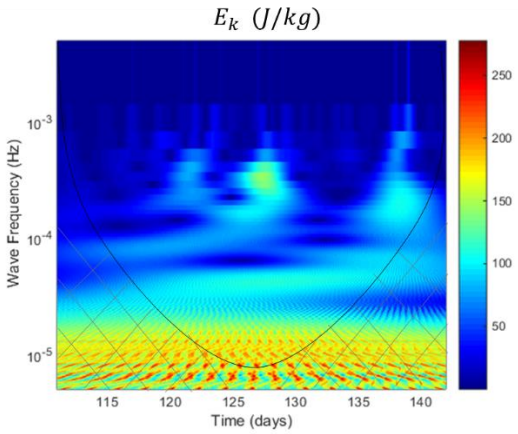

Figure 4: Wavelet power spectrum of kinetic energy density obtained from summed wavelet spectra of averaged velocity squared in between 19-23 km for the month of May 2006. The thick black lines represents the cone of influence and the grey checked region is erroneous data.

From analysing the spectrum, Eulerian wave frequency ω can be identified. Usually, the frequencies with significant spectral power are of the interest because they have large amplitudes (Evan & Alexander 2008; Hankinson et al. 2014b). From the spectrum shown in Figure 4, the waves with significant power are identified using the 95% significance test (Torrence & Compo 1998) based on the red noise spectrum. This method is very common for wavelet analysis in atmospheric sciences. The one drawback of wavelet transform is the loss of spectral accuracy near the ends of the signal which is defined using the cone of influence highlighted in Figure 4. The spectral power outside the cone is usually inaccurate and not considered during the analysis (highlighted by grey checked region). Based on the red noise

spectrum, it is likely that more high frequency waves will be significant as the red noise level at lower frequencies are very high. The yearly mean statistics of occurrence of different waves is shown in Figure 5. It is seen that most common significant waves occurring in this region have periods in between 5 to 30 hours. The least number of significant waves occurred with periods above 60 hours. These results agree with study conducted by Kafando et al. (2016). The mean monthly wave period with highest spectral power is listed in Table 1.

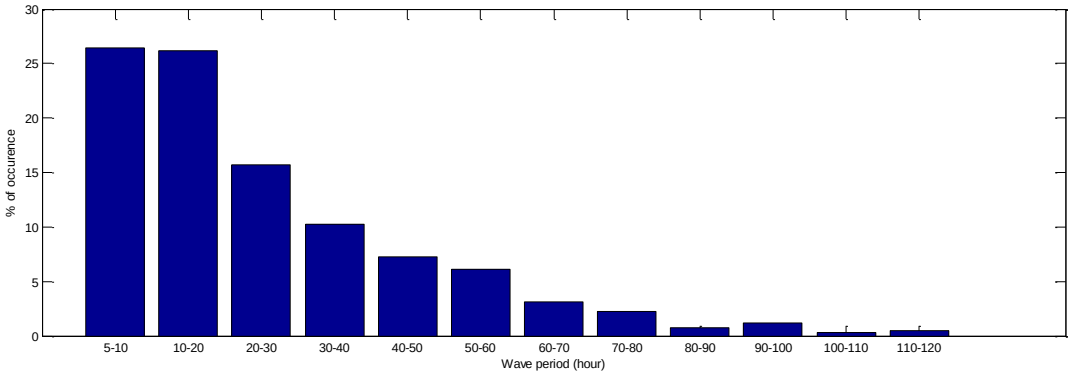

Figure 5: Bar graph showing the yearly averaged percentage of occurrence of the gravity wave periods binned into 12 period ranges. The total number of waves identified were 45,128 with 95% significance power.

Once the Eulerian frequencies are identified as inertia gravity waves, the other properties can be calculated for these waves. The intrinsic frequency can be calculated using the ratio between the kinetic and potential energy. This method has been demonstrated by (Geller & Gong 2010) using the dispersion relations. The expression for this ratio is as shown in equation (6):

$$\frac{\overline{E_k}}{\overline{E_p}} = \frac{\left(1 + \left(\frac{f_e}{\widehat{\omega}}\right)^2\right)}{\left(1 - \left(\frac{f_e}{\widehat{\omega}}\right)^2\right)} \tag{6}$$

The overbars over E_k and E_p represent averaging between an altitude range (19-23 km in this case). The ratio of energy densities varies from 1.5 to 5 during the campaign period with peak values occurring during the wet season. The ratio $\widehat{\omega}/f_e$ varies from 1 to 1.9 which is in agreement with the study conducted by Kafando et al. (2016). The monthly average values of $\widehat{\omega}$ are shown in Table 1 and Figure 7. Using the dispersion relations shown in equations (7) and (8), the horizontal and vertical wavelengths and wavenumbers were calculated (Evan & Alexander 2008; Fritts & Alexander 2003).

$$k_h = \frac{\omega - \widehat{\omega}}{\overline{U}} \tag{7}$$

$$m^2 = \frac{(k^2 + l^2)(N^2 - \widehat{\omega}^2)}{(\widehat{\omega}^2 - f_e^2)} - \alpha^2 \tag{8}$$

where $k_h = \sqrt{k^2 + l^2}$, is the total horizontal wavenumber, $\overline{U}$ is the mean total horizontal velocity $\overline{U} = \sqrt{u^2 + v^2}$, $\alpha^2 = 1/4H_s^2$ where H_s is the density scale height. In order to calculate k and l from k_h, the horizontal propagation direction is needed which can be calculated using the equation (9) (Evan & Alexander 2008; Hankinson et al. 2014b; Kafando et al. 2016).

$$\Phi = \tan^{-1}\left(\frac{\overline{u'T'_{+90}}}{\overline{v'T'_{+90}}}\right) \tag{9}$$

where T'_{+90} is the Hilbert transform of the temperature perturbation signal. From k_h and m, it is possible to calculate the corresponding wavelengths which are shown in Figure 6. The median values of gravity wave properties for each month are listed in Table 1, and variance of wavelengths and horizontal propagation direction is shown in Figure 6 and Figure 8. It can be seen that λ_h varies quite a lot during these months, while λ_v has relatively low variance.

Table 1: Median values of gravity wave properties for each month of wet season calculated in the stratosphere. f_e – earth's inertial frequency, λ_v – vertical wavelength, λ_h - horizontal wavelength, ACW/CW – vertical propagation indicator and Φ – horizontal propagation direction.

	$\widehat{\omega}/f_e$	$\lambda_v\ (km)$	$\lambda_h\ (km)$	$\frac{ACW}{CW}$	Φ (° from east)
January	1.49	1.66	567.82	2.68	-3.68
February	1.67	1.70	374.52	3.45	26.26
March	1.55	1.78	547.63	3.21	24.22
April	1.46	2.37	49.06	2.85	11.31
May	1.65	3.18	334.96	3.86	-1.68
June	1.76	3.67	424.34	2.95	9.85
July	1.54	3.63	1526.57	3.95	20.86
August	1.57	3.31	1026.67	4.12	17.77
September	1	2.09	1583.37	4.03	12.36
October	1.51	0.85	279.8	2.45	-3.15
November	1.48	0.97	446.33	2.09	-5.21
December	1.52	0.89	104.18	2.14	6.95

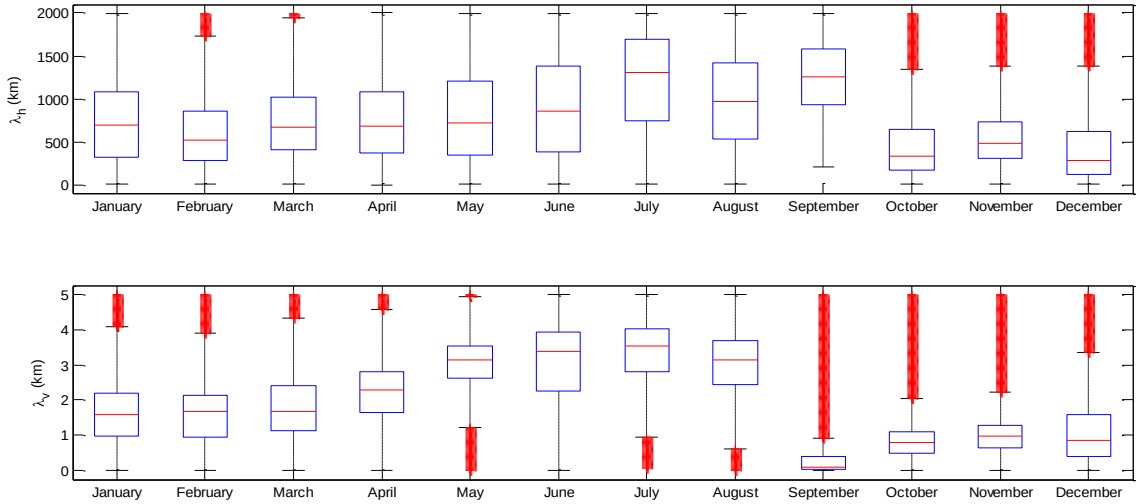

Figure 6: Monthly range and median values of horizontal wavelengths (upper) and vertical wavelengths (lower). The red line inside the box indicates the median value, the top and bottom lines of the box indicates the 25th and 75th percentiles of the samples. The black lines extending outside the box show the further point at which the values is 1.5 times the interquartile values. The outliers shown in red outside these lines.

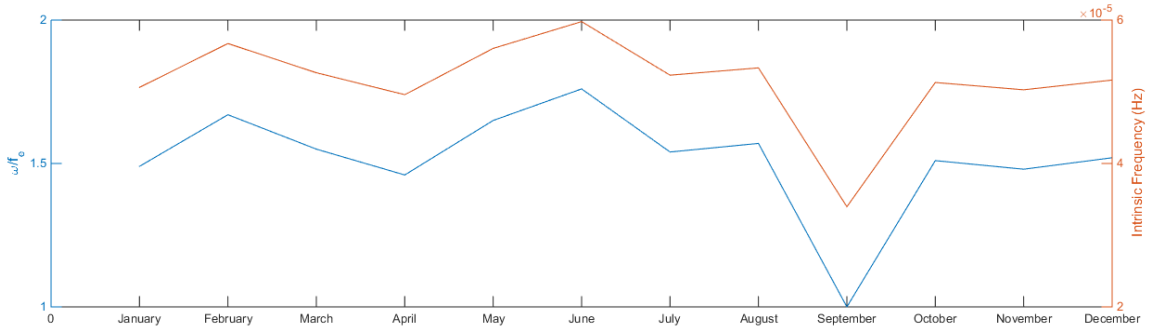

Figure 7: Monthly mean variation of (right vertical axis) intrinsic frequency (Hz) and (left vertical axis) intrinsic frequency-to-earth's inertial frequency ratio.

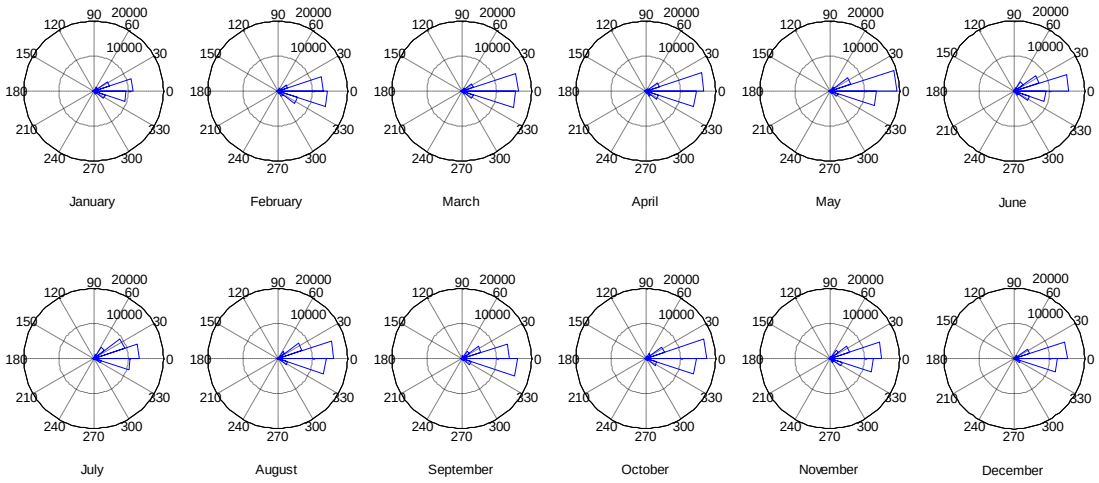

Figure 8: Monthly horizontal phase propagation angle (in degrees) histogram observed in the stratosphere.

The general direction of propagation is mainly eastwards, as shown in Figure 8 with dominant northeast propagation during the wet season. These are aligned mainly with easterlies occurring near the tropopause altitudes driven the Hadley cells circulation in the tropical region (Stull 2011).

Stokes parameters were calculated to determine the vertical propagation direction. They can be calculated using the profile of wind speed perturbations u' and v'. The method is described in (Eckermann & Vincent 1989) which the separates the perturbations into real and imaginary parts over the complete altitude range. This method has been used in various previous studies to calculate the vertical propagation direction (Hankinson et al. 2014b; Pramitha et al. 2016; Kafando et al. 2016). The Fourier transformed perturbations can be expressed as $U_R(m) + iU_I(m)$, and $V_R(m) + iV_I(m)$ are zonal and meridional winds respectively, where they are functions of vertical wavenumber. Stokes parameters are calculated using equations (10) – (13).

$$\mathrm{I} = \mathrm{A}\left[\overline{\mathrm{U}_{\mathrm{R}}^2(m)} + \overline{U_I^2(m)} + \overline{V_R^2(m)} + \overline{V_I^2(m)}\right] \quad (10)$$

$$D = \mathrm{A}\left[\overline{\mathrm{U}_{\mathrm{R}}^2(m)} + \overline{U_I^2(m)} - \overline{V_R^2(m)} - \overline{V_I^2(m)}\right] \quad (11)$$

$$P = 2A\left[\overline{U_R(m)V_R(m)} + \overline{U_I(m)V_I(m)}\right] \quad (12)$$

$$Q = 2A[\overline{U_R(m)V_I(m)} - \overline{U_I(m)V_R(m)}] \quad (13)$$

where m is the vertical wave number, A is a constant and subscripts R and I denote the real and imaginary parts of Fourier transforms. The overbars denote the average of all the profiles available. The clockwise (CW) and anticlockwise (ACW) rotation of horizontal wind perturbations with height can be used to determine the propagation direction (Eckermann 1996). If the ratio of ACW to CW is greater than 1, it can be concluded that direction of propagation is upwards and these can be calculated using equation (14) (Hankinson et al. 2014a).

$$\begin{aligned} \mathrm{CW} &= 0.5[\mathrm{I(m)} - \mathrm{Q(m)}] \\ ACW &= 0.5[I(m) + Q(m)] \end{aligned} \quad (14)$$

The calculated ACW-to-CW ratio varied from 0.5 to 5.4 over the altitude range (15 – 23 km) for each month. The altitudes above 20 km had values higher than 2 in general indicating that major proportion of energy is propagating upwards in stratosphere compared to troposphere. The monthly median values of ACW-to-CW ratios are shown in Table 1 in which it can be seen that wet season has relatively higher values. The frequency occurring local convections can be responsible for increased upward propagation of the energy (Fritts & Alexander 2003). Now that all the required properties are obtain, the ray tracing simulations can be performed in order to determine the source location.

4. Source location identification

The gravity wave properties calculated in the previous section are observed in the stratosphere using the vertical profile measurements. The precise source of the identified waves is yet to be tracked or traced back. This is performed using the Gravity wave Regional Or Global Ray Tracer model (GROGRAT). This model basically applies the EM wave ray tracing method to the gravity waves by modifying the dispersion relations suitable to the application (Marks & Eckermann 1995; Eckermann & Marks 1997). Various studies have used this method to retrieve the source location of the gravity waves (Hankinson et al. 2014b; Pramitha et al. 2016) It solves a nonhydrostatic dispersion relation appropriate for small-amplitude gravity waves on a slowly varying basic flow $\mathbb{U} = (u, v, 0)$ in a rotating, stratified and compressible atmosphere (Marks & Eckermann 1995). GROGRAT model is not valid for high frequency waves for which a threshold has been defined, called critical intrinsic frequency. Therefore, all the waves analysed here are lower than critical intrinsic frequency of $2.698 \times 10^{-3}\ Hz$. The background atmosphere is considered to be slowly variant and therefore, ECMWF ERA-Interim 6-hour ensemble model with grid resolution of $0.75° \times 0.75°$ with 37 altitudes levels was used to provide background variables. This method requires the gradient of background variables to change smoothly in order for the WKB approximation to remain valid which is shown in equation (21). Therefore, as suggested in Marks & Eckermann (1995), a spherical harmonic smoothing has been applied in the horizontal and cubic spline smoothing in the vertical.

The model requires the initial values of k, l, m, x, y and z, along with the initial values of gradients of background variables. The gravity wave analysis described in the previous section provided the wave properties which will be used as initial values. With the ω selected, the corresponding $\hat{\omega}, k, l$ and m was calculated at a particular instance in time. The initial position considered here is the stratospheric altitude point 23 km above Niamey. Using the flat earth coordinate system, the geographical coordinates are converted to local Cartesian coordinate system (Marks & Eckermann 1995). The initial values of gradients are calculated from the ERA-Interim model.

The GROGRAT model is based on dispersive waves in which the frequency of the wave is a function of the wavenumber and the position. The method basically solves six differential equations in order to obtain the wave path in a reverse tracing method. The ray tracing equations are shown from equation (15) to (20).

$$\frac{\mathrm{dx}}{\mathrm{dt}} = U + \frac{k(N^2 - \hat{\omega}^2)}{\hat{\omega}(k^2 + l^2 + m^2 + \alpha^2)} \quad (15)$$

$$\frac{dy}{dt} = V + \frac{l(N^2 - \hat{\omega}^2)}{\hat{\omega}(k^2 + l^2 + m^2 + \alpha^2)} \quad (16)$$

$$\frac{dz}{dt} = -\frac{m(\hat{\omega}^2 - f_e^2)}{\hat{\omega}(k^2 + l^2 + m^2 + \alpha^2)} \quad (17)$$

$$\frac{dk}{dt} = -k\frac{dU}{dx} - l\frac{dV}{dx} - \frac{\left[\left(\frac{dN}{dx}\right)^2 (k^2 + l^2) - \left(\frac{d\alpha}{dx}\right)^2 (\hat{\omega}^2 - f_e^2)\right]}{2\hat{\omega}(k^2 + l^2 + m^2 + \alpha^2)} \quad (18)$$

$$\frac{dl}{dt} = -k\frac{dU}{dy} - l\frac{dV}{dy} - \frac{\left[\left(\frac{dN}{dy}\right)^2 (k^2 + l^2) - \left(\frac{d\alpha}{dy}\right)^2 (\hat{\omega}^2 - f_e^2)\right]}{2\hat{\omega}(k^2 + l^2 + m^2 + \alpha^2)} - \frac{\left[f_e \frac{df_e}{dy}(m^2 + \alpha^2)\right]}{\hat{\omega}(k^2 + l^2 + m^2 + \alpha^2)} \quad (19)$$

$$\frac{dm}{dt} = -k\frac{dU}{dz} - l\frac{dV}{dz} - \frac{\left[\left(\frac{dN}{dz}\right)^2 (k^2 + l^2) - \left(\frac{d\alpha}{dz}\right)^2 (\hat{\omega}^2 - f_e^2)\right]}{2\hat{\omega}(k^2 + l^2 + m^2 + \alpha^2)} \quad (20)$$

where U, V are the background velocities in x, y directions. The Eulerian frequency ω is assumed to be constant throughout the ray path, and this fact is used as a validity check of the integrations (Marks & Eckermann 1995). A fourth order Runge-Kutta method was used for solving the differential equations (15)-(20). The WKB approximation shown in equation (21) is used to determine the end of the ray path.

$$\delta \approx \left|\frac{1}{\mathrm{c_{g_z}} m^2}\frac{dm}{dt}\right| \quad (21)$$

The integration is terminated when $\delta \geq 1$, which happens as $m \to 0$. Waves are reflected in such situations, and reflected waves are not of interest in this case. It is taken in regard that some gravity waves with large δ, may propagate through the atmosphere while violating the WKB approximation, but it is also difficult to analyse and identify the end of ray path in such cases because the ray-tracer method is not valid for cases in which the rate of change of m is too high. Therefore, termination of ray was carried out when WKB is not valid anymore.

The ray tracer has been applied for 240 waves of the identified waves. The initial values for the ray tracers are supplied as explained earlier in this section. The waves simulated were binned based on their termination altitude, which are classified either as high/middle troposphere, low troposphere/near surface or stratosphere. We know that the altitude of tropopause varies with the latitude. This classification is done in order to determine the waves which are likely to be associated with thunderstorms whose vertical extent can vary from 5 km to top of troposphere depending upon the storm strength (Rysman et al. 2017). Depending on the latitude and the season, the tropopause height varies from 8 to 17 km globally (Seidel & Randel 2006). Since, the origin of the waves could be distributed widely, it is sensible to consider the varying tropopause when defining the bins of termination altitudes. Therefore, the monthly mean tropopause height was used to classify the source location into the bins defined earlier. Figure 9 shows the percentage of waves traced back to different type of source locations (shown as total waves). Around 32.01% terminated in the mid/high-troposphere, 32.35% traced back into the lower troposphere and 35.64% terminated in the stratosphere. Previous studies have shown that the source of the gravity waves can occur at any point in the backward ray traced path (Wei & Zhang 2014b; Wei & Zhang 2014a). Considering this, the ray paths were carefully analysed for thunderstorms for waves terminating in the troposphere. In order to identify the waves generated by thunderstorms, the rays penetrating into the troposphere are classified into four types as shown below:

- Type 1 – thunderstorm as the source at the termination point.
- Type 2 – thunderstorm occurring along the path with other source at the termination point.
- Type 3 – thunderstorm at the termination point coinciding with other sources such as mountain.
- Type 4 – no thunderstorm.

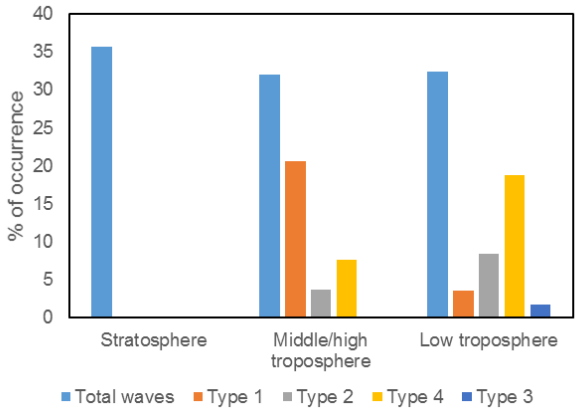

Figure 9: Bar graph showing the occurrences of waves generated from different types of sources.

The ray paths were analysed for thunderstorms in the troposphere along the ray path until the termination point. The source is concluded to be a thunderstorm if a thunderstorm boundary is present within 0.05° radius of the ray path termination point and the termination time occurs within one hour of the event (Hankinson et al. 2014b). The rays which had thunderstorms along the ray path were identified as one of the potential sources or source influencing the existing wave (Wei & Zhang 2014b; Lin & Zhang 2015). The thunderstorm activity is obtained using the ISCCP (International Satellite Cloud Climatology Project) data which uses a cluster of NOAA geostationary and polar orbiting satellites to build global 3-hourly maps of cloud cover and activity.

In Figure 9, it is seen that 64.48% of waves that terminated in mid/high troposphere belonged to type 1 while only 10.97% of waves that terminated in lower troposphere belonged to type 1. 11.68% of waves that terminated in mid/high troposphere belonged to type 2 while 26.12% that terminated in lower troposphere belonged to type 2. The type 2 cases are most likely the waves which already exist in the atmosphere which are influenced by the strong latent heat release from a thunderstorm during its propagation. Since the atmosphere is a continuous fluid, these type of superimposed waves occur very often (Lane & Zhang 2011; Fritts & Alexander 2003). Type 3 are the cases when a thunderstorm was identified at the termination point but the location also coincided with mountains and terrains and 5.5% of rays penetrating into lower troposphere had this ambiguity. Quite a number of waves penetrating into the troposphere were identified to be generated from other sources with no observable influence by the thunderstorms as shown type 4 in Figure 9. It is also to be noted that the gravity waves generated by type 1 may also be influenced by other sources along the ray path (propagation effects) which are extremely difficult to analyse given the limited observational capacity and is beyond the scope of this study.

The trajectories of the waves associated with type 1 and type 2 sources are shown in Figure 10. Most of the type 1 sources are located in the tropical region with propagation time range of 1 to 4 days. These waves are most likely generated by the strong convection activity in the Hadley cells (Stull 2011) which is represented by bright yellow bands in Figure 10b. There are regions over the Atlantic Ocean in the mid-latitudes of southern hemisphere with strong thunderstorm activity which can be seen in Figure 10b (bright yellow band) which are also responsible for some of the type 1 and type 2 waves. The spontaneous balance adjustments which predominantly occurs in mid-latitudes can also be the origins of the waves which have traced back to those regions. Since, the balance adjustments are highly spontaneous and continuous it is extremely difficult to realise them in the observations. Previous studies have discussed the coexistence of waves generated by convection and balance adjustments (Wei & Zhang 2014b) by performing simulations. However, since the thunderstorms were identified along the path; it cannot be ignored as a potential source of wave. Therefore, the waves traced back to mid-latitudes have the ambiguity in identifying the source. This issue of ambiguity is definitely one of major concerns to be addressed in the future.

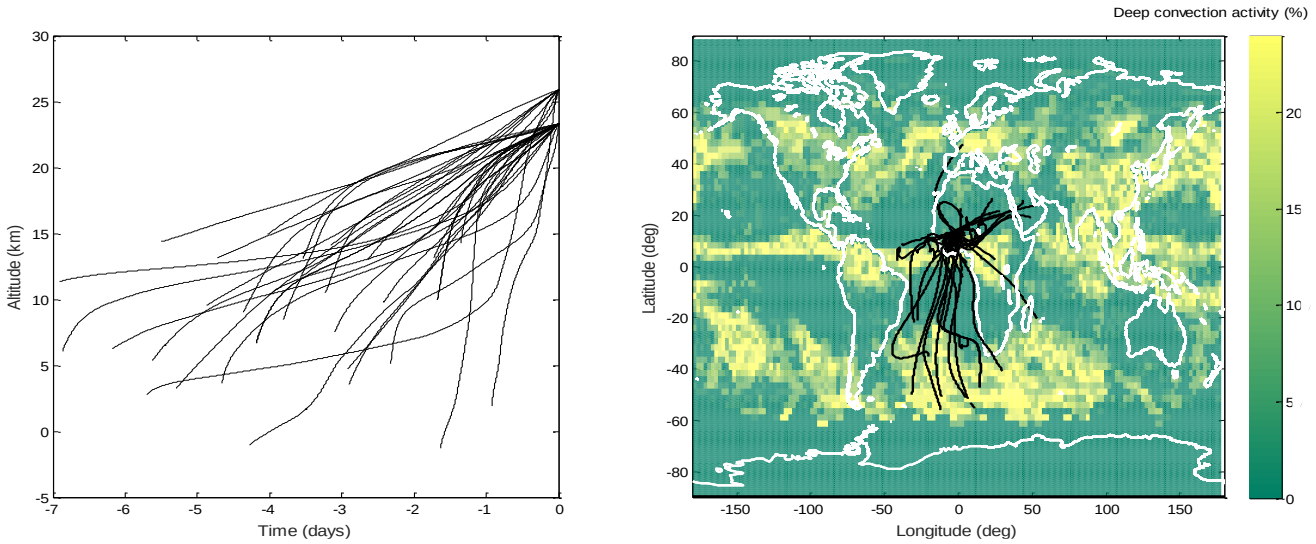

Figure 10: GROGRAT ray tracing results for thunderstorm generated gravity waves path a) altitude-back time plot and b) ray paths (black lines) shown in a geographical map shown along with annual mean deep convection activity during RADAGAST campaign obtained from ISCCP database.

The waves associated with thunderstorms mainly have period from 20 to 40 hours. The horizontal phase speeds at the source point vary from 2 to 20 m/s with highest occurrence at 3 m/s and vertical phase speeds vary from 0.02 to 0.12 m/s with a peak occurring at 0.04 m/s as shown in the Figure 11a and b. The vertical wavelengths at the source point are reasonably consistent with the stratospheric spectrum analysis using the radiosonde observation. The horizontal wavelength varies from 50 to 1000 km with peak at 600 km and vertical wavelength varies from 2 to 15 km with peak at 6 km as shown in Figure 12c and d. The identification of source spectral characteristics were performed in order to develop models based on thunderstorm properties (such as latent heat release) in future.

Previous studies have suggested that the wave properties at the source are correlated with the convective heating (Beres et al. 2004). In this study, it was not possible to conclude any definitive relationship between latent heat of thunderstorms and wave properties because of lack of spatial and temporal geo-collocated data of latent heat distribution. Currently, Tropical Rainfall Monitoring Mission (TRMM) is the only provider of global latent heat estimations, which was not sufficient in this particular study. There is a strong need for increase in the global latent heat estimations which is considered to be one of the future studies following this.

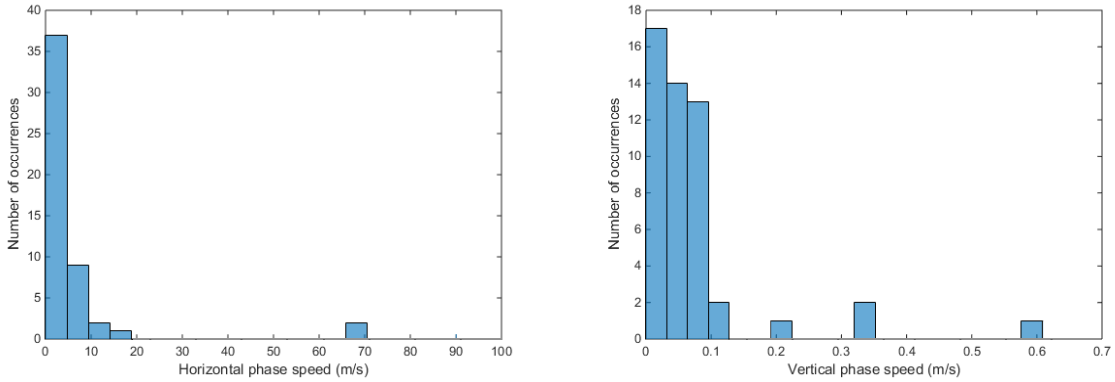

Figure 11: Histograms of a) horizontal phase speed and b) vertical phase speed at the source point of type 1 waves associated with thunderstorms.

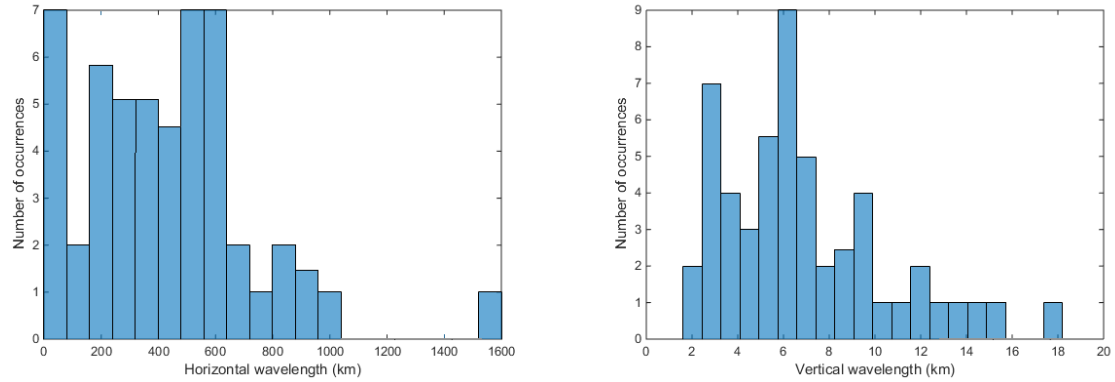

Figure 12: Histograms of c) horizontal wavelength and d) vertical wavelength at the source point of type 1 waves associated with thunderstorms.

Lastly, there are 26.41% cases in which the rays terminated in the troposphere but they were not in range of any thunderstorm clouds. There could be numerous sources for these waves such as mountain (Fritts & Nastrom 1992), jet-fronts and balance adjustments (Reeder & Griffiths 1996; Plougonven & Zhang 2014) (especially in extra-tropical region) and shear instability (Fritts & Alexander 2003; Pramitha et al. 2015; Fritts 1982; Bühler & McIntyre 1999). Since the local data of wind shear (which is known to be one of the sources of gravity waves) was unavailable for those locations, it was not possible to conclude or analyse those waves any further and is beyond the scope of this study.

There are other waves which have terminated in the stratosphere with occurrence rate of 36.47%. It is difficult to analyse these waves because there different possibilities for the existence and propagation: 1) they are generated above tropopause near the inversion layer due to strong wind shear, and 2) they are generated in the higher atmosphere propagating downwards, and reflected back by the inversion layer. The waves with periods from 40 to 60 hours are most frequent with mean horizontal phase speeds from 7 – 20 m/s. It is not in the scope of this study to analyse these waves further, which will need more satellite based local data.

5. Conclusions

In the current study, an attempt was made to determine the thunderstorm generated gravity waves observed over Niamey, Niger station. The initial part of the study used the radiosonde measurements of wind speed and temperature to identify the gravity waves and retrieve their properties. The wavelet transform method was very effective in identifying the range of waves present in the spectrum with different range of spectral powers. A range of wave periods were observed from 7 to 50 hour periods, and waves with periods from 5 - 30 hours having most 95% significant spectral power. The monthly mean intrinsic frequency-to-inertial frequency ratio calculated using energy densities varied from 1 to 1.9. After calculating the horizontal propagation direction, the dispersion relations were used to obtain the wavenumbers. The vertical wavelength varied from 0.9 to 3.7 km while the horizontal wavelength had much wider range from 50 to 1500 km. The general horizontal propagation direction was eastwards but the dominant direction of propagation was towards northeast during the wet season. This is probably due to strong winds from the South Atlantic Ocean. The calculated ACW-to-CW ratio varied from 0.5 to 5.4 over the altitude range (15 – 23 km) for each month. The altitudes above 20 km had values higher than 2 in general indicating that major proportion of energy is propagating upwards in stratosphere compared to troposphere.

GROGRAT model was applied to trace back the ray path to determine the source of the waves identified before. Using the calculated gravity wave properties, 240 rays were simulated out of which 32.01% terminated in the mid/high troposphere (4 – 18 km), 35.64 % were terminated above 18 km, which could mean that either they reflected waves which have source in the higher atmosphere or waves generated from wind shear above tropopause. Also, 32.35% of waves were traced back to lower troposphere below 4 km. Out of the waves terminated in mid/high troposphere; 64.48% were tracked to be originating from thunderstorms and out of waves terminated in lower troposphere; 10.97% were tracked to be originating from thunderstorms as verified using ISCCP global maps. The gravity waves associated with thunderstorms had mean wave periods from 20 to 40 hours with horizontal phase speeds varying from 2 to 20 m/s and vertical phase speeds varying from 0.02 to 0.12 m/s. The vertical wavelengths at the source location varied from 2 to 15 km and horizontal wavelengths varies from 50 to 1000 km. Most of type 1 sources were located in the tropical region where strong thunderstorms occur in the Hadley cells. It was surprising that some of thunderstorm generated waves observed at Niamey were generated from South Atlantic Ocean with mean propagation distance of 5000 km and propagation duration of 2 to 4 days. These waves from originating in mid-latitudes may also be originating from jet-front systems or balance adjustments which could not isolated and verified in the current study. Therefore we conclude these events to be potential sources for the waves seen at Niamey.

This study highlighted that the West African climate has very wide span of geographical coupling as seen in previous section. Not only the observed waves were generated by thunderstorms occurring within 100 to 500 km, but also thunderstorms occurring 5000 km away which are also affected by other circulation effects such as geostrophic adjustment etc. This emphasises the complex coupling of middle atmosphere with upper and lower atmosphere in this region. The future works for this study is to aim for developing a parameterisation between the thunderstorm properties such as latent heat release and wind anomalies and gravity waves that are generated by them. Therefore, the further study is required to realise the thunderstorm properties

in higher temporal and spatial resolution along the amplitude tracked ray tracing of the identified gravity waves.

Acknowledgements

We thank Nanyang Technological University for providing the opportunity for this research. We appreciate and are grateful for ARM, NOAA and ECMWF for providing the data for free on their websites for research purposes.

References

Beres, J.H., Alexander, M.J. & Holton, J.R., 2004. A Method of Specifying the Gravity Wave Spectrum above Convection Based on Latent Heating Properties and Background Wind. *Journal of Atmospheric Sciences*, 61.

Blanc, E. et al., 2014. Ten year observations of gravity waves from thunderstorms in western Africa. *Journal of Geophysical Research Atmospheres*, 119(11), pp.6409–6418.

Bühler, O. & McIntyre, M.E., 1999. On Shear-Generated Gravity Waves that Reach the Mesosphere. Part II: Wave Propagation. *Journal of the Atmospheric Sciences*, 56, pp.3764–3773.

Chun, H.-Y. & Baik, J.-J., 1998. Momentum flux by thermally induced internal gravity waves and its approximation for large-scale models. *Journal of Atmospheric Sciences*, 55.

Clarke, T.L., Hauf, T. & Kuettner, J.P., 1986. Convectively forced internal gravity waves: results from two-dimensional numerical experiments. *Quarterly Journal of the Royal Meteorological SocietyQuarterly Journal of the Royal Meteorological Society*, 112.

Curry, M.J. & Murty, R.C., 1974. Thunderstorm-Generated Gravity Waves. *Journal of the Atmospheric Sciences*, 31(5), pp.1402–1408.

Eckermann, S.D., 1996. Hodographic analysis of gravity waves: Relationships among Stokes parameters, rotary spectra and cross-spectral methods. *Journal of Geophysical Research*, 101.

Eckermann, S.D. & Marks, C.J., 1997. GROGRAT: A new model of the global propagation and dissipation of atmospheric gravity waves. *Advances in Space Research*, 20(6), pp.1253–1256. Available at: http://www.sciencedirect.com/science/article/pii/S0273117797007801.

Eckermann, S.D. & Vincent, R.A., 1989. Falling sphere observations of anisotropic gravity wave motions in the upper stratosphere over Australia. *Pure and Applied Geophysics PAGEOPH*, 130(2–3), pp.509–532.

Evan, S. & Alexander, M.J., 2008. Intermediate-scale tropical inertia gravity waves observed during the TWP-ICE campaign. *Journal of Geophysical Research Atmospheres*, 113(14).

Evan, S., Alexander, M.J. & Dudhia, J., 2012. Model Study of Intermediate-Scale Tropical Inertia–Gravity Waves and Comparison to TWP-ICE Campaign Observations. *Journal of the Atmospheric Sciences*, 69(2), pp.591–610. Available at: http://journals.ametsoc.org/doi/abs/10.1175/JAS-D-11-051.1 [Accessed December 28, 2016].

Fritts, D.C., 1982. Shear Excitation of Atmospheric Gravity Waves. *Journal of the Atmospheric Sciences*, 39(9), pp.1936–1952. Available at: http://journals.ametsoc.org/doi/abs/10.1175/1520-0469(1982)039%3C1936:SEOAGW%3E2.0.CO;2.

Fritts, D.C. & Nastrom, G.D., 1992. Sources of mesoscale variability of gravity waves. I - Topographic excitation. II - Frontal, convective, and jet stream excitation. *Journal of the atmospheric*, 49(2), pp.111–127.

Fritts, D.C.D.C.D.C. & Alexander, M.J., 2003. Gravity Wave Dynamics and Effects in the Middle Atmosphere. *Reviews of Geophysics*, 41(1), pp.1–64. Available at: http://www.agu.org/pubs/crossref/2003/2001RG000106.shtml%5Cnhttp://www.agu.org/journals/rg/rg0301/2001RG000106/.

Geller, M.A. & Gong, J., 2010. Gravity wave kinetic, potential, and vertical fluctuation energies as indicators of different frequency gravity waves. *Journal of Geophysical Research Atmospheres*, 115(11), pp.1–8.

Hankinson, M.C.N., Reeder, M.J. & Lane, T.P., 2014a. Gravity waves generated by convection during TWP-ICE: 2. High-frequency gravity waves. *Journal of Geophysical Research: Atmospheres*, 119(9), pp.5257–5268. Available at: http://doi.wiley.com/10.1002/2013JD020726.

Hankinson, M.C.N., Reeder, M.J. & Lane, T.P., 2014b. Gravity waves generated by convection during TWP-ICE: I. Inertia-gravity waves. *Journal of Geophysical Research: Atmospheres*, 119(9), pp.5269–5282. Available at: http://doi.wiley.com/10.1002/2013JD020724.

Hima Bindu, H. et al., 2016. Characteristics of cyclone generated gravity waves observed using assimilated WRF model simulations over Bay of Bengal. *Atmospheric Research*, 180, pp.178–188. Available at: http://linkinghub.elsevier.com/retrieve/pii/S0169809516301405 [Accessed December 28, 2016].

Jewtoukoff, V., Plougonven, R. & Hertzog, A., 2013. Gravity waves generated by deep tropical convection: Estimates from balloon observations and mesoscale simulations. *Journal of Geophysical Research Atmospheres*, 118(17), pp.9690–9707.

Kafando, P., Chane-Ming, F. & Petitdidier, M., 2008. Climatology of gravity wave activity during the West African Monsoon. *Annales Geophysicae*, 26(12), pp.4081–4089.

Kafando, P., Chane-Ming, F. & Petitdidier, M., 2016. Stratospheric variability of wave activity and parameters in equatorial coastal and tropical sites during the West African monsoon. *Climate Dynamics*, 47(11), pp.3433–3456.

Kim, Y.., Eckermann, S.D. & Chun, H.-Y., 2003. An overview of the past, present and future of gravity-wave drag parametrization for numerical climate and weather prediction models. *Atmosphere-Ocean*, 41.

Lane, T.P. & Moncrieff, M.W., 2008. Stratospheric Gravity Waves Generated by Multiscale Tropical Convection. *Journal of the Atmospheric Sciences*, 65(8), pp.2598–2614. Available at: http://journals.ametsoc.org/doi/abs/10.1175/2007JAS2601.1 [Accessed December 28, 2016].

Lane, T.P. & Zhang, F., 2011. Coupling between Gravity Waves and Tropical Convection at Mesoscales. *Journal of the Atmospheric Sciences*, 68(11), pp.2582–2598. Available at: http://journals.ametsoc.org/doi/abs/10.1175/2011JAS3577.1 [Accessed December 28, 2016].

Lin, Y. & Zhang, F., 2015. Tracking gravity waves in baroclinic jet-front systems. *Journal of Advances in Modeling Earth Systems*, 7(1), pp.67–91.

Marks, C.J. & Eckermann, S.D., 1995. A Three-Dimensional Nonhydrostatic Ray-Tracing Model for Gravity Waves: Formulation and Preliminary Results for the Middle Atmosphere. *Journal of the Atmospheric Sciences*, 52(11), pp.1959–1984. Available at: http://journals.ametsoc.org/doi/abs/10.1175/1520-0469(1995)052%3C1959:ATDNRT%3E2.0.CO;2.

Morrison, H. & Grabowski, W.W., 2013. Response of Tropical Deep Convection to Localized Heating Perturbations: Implications for Aerosol-Induced Convective Invigoration. *Journal of the Atmospheric Sciences*, 70(11), pp.3533–3555. Available at: http://journals.ametsoc.org/doi/abs/10.1175/JAS-D-13-027.1 [Accessed December 28, 2016].

Plougonven, R., Hertzog, A. & Alexander, M.J., 2015. Case studies of nonorographic gravity waves over the Southern Ocean emphasize the role of moisture. *Journal of Geophysical Research Atmospheres*, 120(4), pp.1278–1299.

Plougonven, R. & Zhang, F., 2013. Internal gravity waves from atmospheric jets and fronts. *Reviews of Geophysics*, 52, pp.33–76.

Plougonven, R. & Zhang, F., 2014. Internal gravity waves from atmospheric jets and fronts. *Reviews of Geophysics*, 52(1), pp.33–76.

Pramitha, M. et al., 2015. Evidence for tropospheric wind shear excitation of high-phase-speed gravity waves reaching the mesosphere using the ray-tracing technique. *Atmospheric Chemistry and Physics*, 15(5), pp.2709–2721.

Pramitha, M. et al., 2016. Identification of inertia gravity wave sources observed in the troposphere and the lower stratosphere over a tropical station Gadanki. *Atmospheric Research*, 176–177, pp.202–211. Available at: http://linkinghub.elsevier.com/retrieve/pii/S0169809516300515 [Accessed December 28, 2016].

Reeder, M.J. & Griffiths, M., 1996. Stratospheric inertia-gravity waves generated in a numerical model of frontogenesis. II: Wave sources, generation mechanisms and momentum fluxes. *Quarterly Journal of the Royal Meteorological Society*, 122(533), pp.1175–1195.

Rysman, J., Claud, C. & Delanoë, J., 2017. Monitoring Deep Convection and Convective Overshooting From 60 ° S to 60 ° N Using MHS : A Cloudsat Calipso-based Assessment. *IEEE Geoscience and Remote Sensing Letters*, 14(2), pp.159–163.

Salby, M.L. & Garcia, R.R., 1987. Transient response to localized episodic heating in the tropics. Part1: excitation and short-time near field behavior. *Journal of Atmospheric Sciences1*, 44(2).

Seidel, D.J. & Randel, W.J., 2006. Variability and trends in the global tropopause estimated from radiosonde data. *Journal of Geophysical Research*, 111(April), pp.1–17.

Stull, R., 2011. *Meteorology for Scientists and Engineers* 3rd ed., Canada: University of British Columbia.

Torrence, C. & Compo, G.P., 1998. A Practical Guide to Wavelet Analysis. *Bulletin of the American Meteorological Society*, 79(1), pp.61–78.

Troyan, D., 2012. *Merged sounding value-added product*, Available at: http://www.arm.gov/publications/tech_reports/doe-sc-arm-tr-087.pdf.

Wang, C., 2005. A modeling study of the response of tropical deep convection to the increase of cloud condensation nuclei concentration: 1. Dynamics and microphysics. *Journal of Geophysical Research Atmospheres*, 110(21), pp.1–16.

Wang, X. & Zhang, M., 1999. The coupling of mixed Rossby-gravity waves with diabatic heating during the TRMM-KWAJEX field campaign. *Geophysical Research Letters*, (July), pp.166–169.

Wei, J. & Zhang, F., 2014a. Mesoscale Gravity Waves in Moist Baroclinic Jet–Front Systems. *Journal of the Atmospheric Sciences*, 71(3), pp.929–952. Available at: http://journals.ametsoc.org/doi/abs/10.1175/JAS-D-13-0171.1.

Wei, J. & Zhang, F., 2014b. Tracking gravity waves in moist baroclinic jet-front systems. *Journal of Advances in Modeling Earth Systems*, pp.67–92.

Yiğit, E. et al., 2016. A review of vertical coupling in the Atmosphere–Ionosphere system: Effects of waves, sudden stratospheric warmings, space weather, and of solar activity. *Journal of Atmospheric and Solar-Terrestrial Physics*, 141, pp.1–12. Available at: http://linkinghub.elsevier.com/retrieve/pii/S1364682616300426 [Accessed September 15, 2016].

Yiğit, E. & Medvedev, A.S., 2015. Internal wave coupling processes in Earth's atmosphere. *Advances in Space Research*, 55(4), pp.983–1003. Available at: http://linkinghub.elsevier.com/retrieve/pii/S0273117714007236 [Accessed December 28, 2016].